




# Ice Reconnaissance Data Processing Under Low Quality Source Images

Andrey Timofeev<sup>1</sup> , Aleksander Titov<sup>2</sup>  , and Denis Groznov<sup>1</sup> 

<sup>1</sup> LLP “EqualiZoom”, Astana, Kazakhstan

<sup>2</sup> Peter the Great St. Petersburg Polytechnic University, Polytechnicheskaya 29,  
195351 St. Petersburg, Russia  
titov\_ab@spbstu.ru

**Abstract.** The ice reconnaissance task is extremely important for maritime logistics in high latitudes as the results of its solution are the basis for the development of rational ship routes in high latitudes areas. The intermediate result of ice reconnaissance is a huge corpus of aerial survey data of poor quality. Since the amount of aerial survey data is extremely high, it is necessary to ensure the maximum efficiency of its data processing under low quality source images. The paper considers the issues of highly efficient automation of ice reconnaissance data processing based on the use of machine learning methods. In particular, the problem of automatic classification of the sea-ice floe size distribution (FSD) type for a three-class model based on aerial survey data is solved. The case of low-quality images is considered, which is a usual situation for meteorological conditions of the Far North. We have proposed a new classification method of FSD type based on aerial survey data processing using machine learning methods which is quite effective for low quality images processing. Also, an original feature space, which ensured the efficiency of this classification method, was proposed. The method has shown its high efficiency in testing it on Data Set, compiled from real low quality images (high blurriness, fuzziness, presence of meteorological disturbances). The developed algorithm is based on multi-class SVM and is extremely undemanding to computing resources, so it can be placed onboard an ice reconnaissance UAV.

**Keywords:** Sea-ice floe size distribution · Ice reconnaissance · Image classification · Multi-class SVM · Image histogram · Blurry images · Sea-ice type classification

## 1 Introduction

Shipping routes in the Northern latitudes, including the Northern Sea Route, do not have a permanent geographical reference and are formed based on a set of hydro-meteorological information, which comes to the ship. As a rule, the total length of the route, in this case, is a variable value, since throughout the route the vessel is affected by different from each other ice conditions. In this case, the tortuosity coefficient always exceeds unity, and additional increase in route length of the route in old ice due to their circumvention is 10–30% [1]. When laying routes in the Northern latitudes, the concept of a rational

route, which best meets some formal criterion (for example: route length, travel time along the route, fuel economy and others) plays an important role [2]. The main criterion used when constructing a rational route in the Northern latitudes is the total time spent on its passage time. A rational route is usually laid through the zones where: total ice cohesion is minimal, young ice forms prevail, and ice torsion is minimal. All this information can be obtained operatively only from ice reconnaissance data. Thus, without taking into account hydro-meteorological information, which is mainly the result of ice reconnaissance, the construction of a rational route is fundamentally impossible. Therefore, the role of ice reconnaissance in the set of tasks for providing logistics in northern latitudes is extremely important. The main navigational characteristic to be monitored during ice reconnaissance is the “ice cohesion” characteristic. Ice cohesion is the ratio of the area of ice in area  $X$  to the total area of this area, expressed in fractions or scores [3]. Let us denote this parameter by the symbol  $S(X)$ . It is the parameter  $S(X)$  that cardinaly affects the ability to navigate in a particular area of the sea [3]. More precisely: the resistance of broken ice increases in proportion to the value of  $(2 - S(X)) \cdot S^2(X)$  [3]. Somewhat differently, but close in meaning, ice cohesion can be described by the concept of “floe size distribution” (FSD) [4]. There are many papers devoted to the study of FSD, e.g., [4–11], from which it follows that this FSD is well approximated by the power law. At the same time, some works consider more complex models, such as mix of power law and gaussian law or the mix of two power laws with different parameters. Depending on the type of FSD, the ice is classified into classes according to the  $N$  point system. That is, solid ice gets the maximum number of points ( $N$ ), and sparse ice gets the minimum number of points. Different applications of the FSD concept imply different values of  $N$ . For example, in [12]  $N = 10$ , and in [4]  $N = 3$ . From a practical point of view, it is the ice cohesion score assigned to a particular area  $\Xi_i$  of the sea surface with an ice cohesion value  $S[\Xi_i]$  that is important. Let's denote this value by  $\gamma_i$ ,  $\gamma_i = \{1, \dots, N\}$ . In practice, the value of  $\gamma_i$  is calculated using the processing (manual or automatic) of some image  $I(\Xi_i)$  of the surface area  $\Xi_i$ . The image  $I(\Xi_i)$  can be made in one or another spectral range, this image can be obtained by one or another means of aerial photography. The data processing procedure  $D$ , which calculates the value  $\gamma_i$  based on  $I(\Xi_i)$ , in fact, maps the set of all possible images of different parts of the sea surface (which form the set  $\Xi$ ), onto the set  $\{1, \dots, N\}$ . That is:

$$\begin{aligned} \Xi &\xrightarrow{D} \{1, \dots, N\}. \\ \gamma &= D(I(\Xi_i)) \in \{1, \dots, N\}, I(\Xi_i) \in \Xi. \end{aligned}$$

In fact,  $D$  is a classifier. Depending on the value of  $\gamma_i$ , the decision is made to include or not to include the section  $\Xi_i$  in the ship's route. It follows from this definition that  $\gamma_i$  is a discrete (otherwise coarse) descriptor of the value  $S[\Xi_i]$ .

The efficiency of  $D$  classifier implementation directly affects the correctness of determining the value of  $\gamma$ , and consequently, the efficiency of ice reconnaissance data implementation. Many works are devoted to methods of construction of the classifier  $D$ , for example [13–25]. Different methods of image processing are traditionally used, but the main accent is made on studying the boundaries of elements of a scene, which represents an image. In this direction, considerable progress has been made, including the use of

the fashionable concept of Deep Learning [19]. In this work, Deep Convolutional Neural Network is successfully used to process ice reconnaissance data.

Against the background of huge recent achievements in the field of ice reconnaissance data, the problem remains the construction of such a classifier  $D$ , which would be able to work with images of very low quality. Namely, low-quality ice images are not uncommon when operating in the High Latitudes using UAVs equipped with visible range sensors, which is due to the chronically difficult weather conditions of this region. The images practically used to determine  $\gamma$  are often very blurry and highly noisy. As a rule, traditional image processing methods based on the analysis of image element boundaries (in fact: local contrast gradients and Hessians) prove ineffective when processing blurred images [26]. In addition, developers are often faced with the problem of a training corpus of small volume. Also relevant is the task of ensuring the processing of ice reconnaissance data directly on board the UAV, which imposes additional requirements for optimizing the computational complexity of the algorithms for determining  $\gamma$ .

Therefore, the main goal of this paper is to develop a classifier  $D$  that would be operable for low-quality image processing, remain operable for training on a small volume image body, and be adaptable for implementation in the onboard complex of a small UAV.

## 2 Materials and Methods

### 2.1 Description of the Features Space Used

For automatic classification of images, explicitly or implicitly, some numerical characteristics of the image are calculated, which informatively characterize the image. Ideally, they are invariant to scale, rotation and illumination, and also have a significantly smaller dimensionality than the original image. These features are called features. Typical examples of features are: histograms, image pixel intensity, contrast gradient, contrast Hessian, SIFT-descriptors (spatial histogram of the image gradients), HOG (histogram of oriented gradients) and so on. The main idea underlying the proposed method is to form such features that characterize large fragments of the analyzed image, avoiding the use of features that characterize small details. We will call the feature of the first type – global and the feature of the second type – local. The main task of ice reconnaissance is to estimate the FSD type for quite large fragments of sea surface. This problem can be solved by different methods, which allow the use of both global and local features. For example, in [8, 11, 21] both types of features are considered, and in [4, 19, 24] preference is given to the study of local features. For the case of blurred, noisy images considered in this paper, the use of fine details of the image, for example, based on the calculation of contrast gradients and Hessians, is problematic. In other words, in this case, computing local features involves unacceptable errors. Local features computed in this way are uninformative and therefore unsuitable for solving the problem of FSD classification or other concepts characterizing FSD, in particular, for determining the parameter  $\gamma$ . On the other hand, global features are less dependent on the parameters of image blurring (although there is such dependence). The stability of global features is

largely determined by the radius of correlation of the image: the larger this value is, the more stable the global features are to the effects of blurring and noisiness factor.

That is why this paper focuses on the use of global features. Initially, a fairly wide set of features was considered: more than thirty. At subsequent stages, this set was reasonably narrowed down by selecting the most informative features. Several methods were used, including three so-called “filtering” methods: chi-square, Pearson correlation and analysis of variance (ANOVA), as well as adaptive method of backward elimination. As a result, the following set of features was obtained:

$$f_{\Xi} = (\mathbf{E}[I(\Xi)], |\Xi|, ST[I(\Xi)], H_m[I(\Xi)], r_{\Xi}, E(A_{\Xi}|x \geq r_{\Xi}), st(A_{\Xi}|x \geq r_{\Xi}))$$

Here:

- $I(\Xi) = \{i_x|x \in X_{I(\Xi)}\}$ - image of  $\Xi$ ,  $x$ -coordinates,  $X_{I(\Xi)}$ - image  $I(\Xi)$  coordinate set,  $i_x$ - intensity in image point with coordinates  $x$ ;
- $\mathbf{E}[I(\Xi)] = \sum_{x \in X_{I(\Xi)}} i_x |I(\Xi)|^{-1}$ , hereinafter, the entry  $|B|$  denotes the power of the set  $B$ ;
- $|I(\Xi)| = \max_{x \in X_{I(\Xi)}} (i_x) - \min_{x \in X_{I(\Xi)}} (i_x)$ ;
- $ST(\Xi) = \sqrt{\sum_{x \in X_{I(\Xi)}} (i_x - \mathbf{E}[I(\Xi)])^2 |X_{I(\Xi)}|^{-1}}$ ;
- $H_m(\Xi)$ - histogram of  $I(\Xi)$  with  $m$  bins;
- $A_{\Xi}(l)$ -autocorrelation function of the  $I(\Xi)$  (averaged over different slices),  $l \in (0, d)$ - pixel shift;  $d$  is determined by the size of the  $I(\Xi)$ ;
- $r_{\Xi}$  - radius correlation of  $I(\Xi)$ (averaged over different slices);
- $E(A_{\Xi}(l)|l \in (r_{\Xi}, d)) = \sum_{l \geq r_{\Xi}} A_{\Xi}(l)(d - r_{\Xi})^{-1}$ ;
- $st(A_{\Xi}|x \geq r_{\Xi}) = \sqrt{\sum_{l \geq r_{\Xi}} (A_{\Xi}(l) - E(A_{\Xi}(l)|l \geq r_{\Xi}))^2 ((d - r_{\Xi})(d - r_{\Xi} - 1))^{-1}}$ .

In numerical studies it was assumed that  $m = 14$ . The features  $f_{\Xi}$  are defined in the corresponding feature space  $\mathbf{F}$ , consisting of real vectors of length 20.

## 2.2 Description of the Data Set Used

To set up and test the proposed classifier, we used a Data Set specially created for this purpose. This Data Set included, according to the classification from [4], images of three FSD distribution classes, namely: “Pack Ice”, “Marginal Ice Zone” and “Open Ocean” (Fig. 1). At statement of the problem the variant of use, so-called, “background” class was quite consciously excluded. Images of all three classes were collected from open sources. Then, in order to simulate the influence of a complex meteorological situation, the images were subjected to the procedure of artificial noising by spatially correlated noise and smoothing by a Gaussian filter.

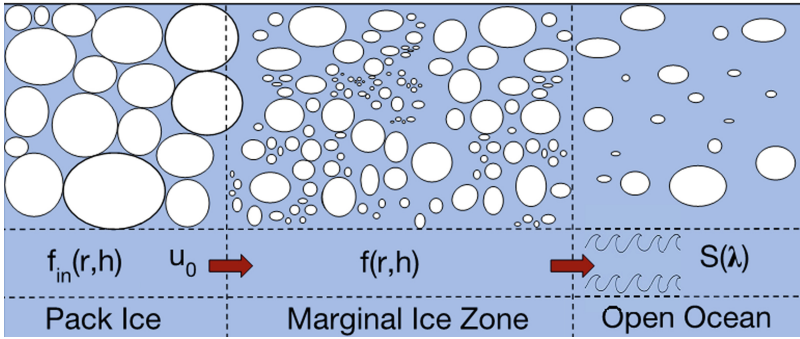


**Fig. 1.** FSD types used in this study. This figure is taken from the article

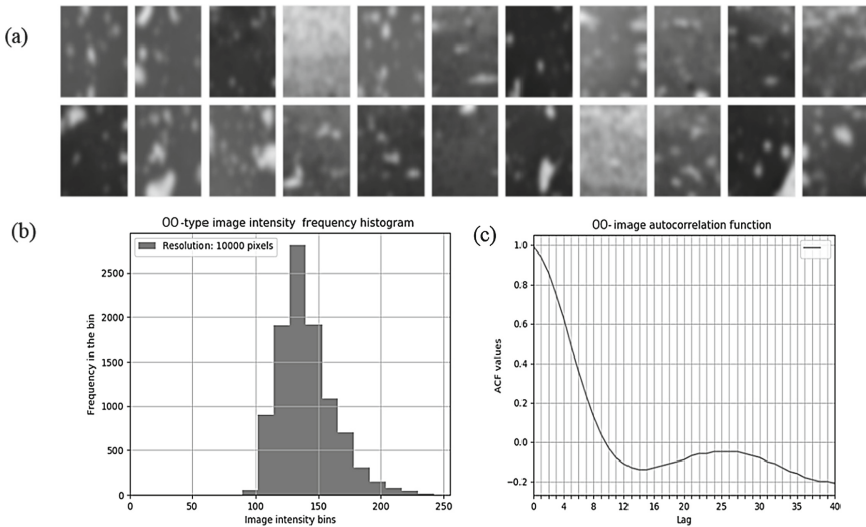


**Fig. 2.** Class “Open Ocean” (OO). (a) Typical sample images from the OO class. (b) Intensity histogram plotted over the entire typical image from the OO class. (c) Typical autocorrelation function of an OO- image (averaged over different slices)

Data Set was obtained, in which class PI (“Pack Ice”) corresponds to 96 samples, class MIZ (“Marginal Ice Zone”) corresponds to 76 samples, class OO (“Open Ocean”) corresponds to 192 samples. Figure 2 shows the information on the class “Open Ocean”. Figure 3 shows information on class “Marginal Ice Zone”, and Fig. 4 shows information on class “Pack Ice”. It can be seen from the figures that the video material is of very low quality: ice edges are very blurred, contrast is low. But it is images of such quality that are typical when using small UAVs in the difficult meteorological conditions of the High Latitudes.

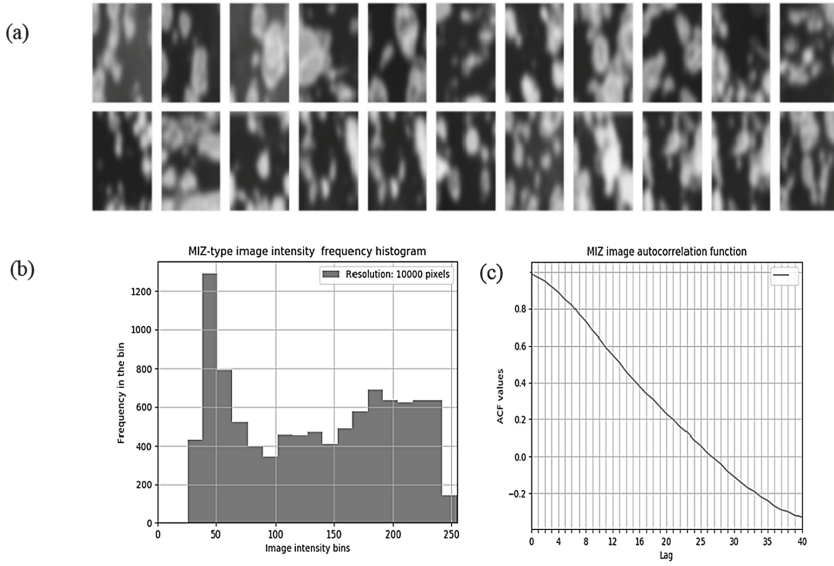


**Fig. 3.** Class “Marginal Ice Zone” (MIZ). (a) Typical sample images from the MIZ class. (b) Intensity histogram plotted over the entire typical image from the MIZ class. (c) Typical autocorrelation function of MIZ- image (averaged over different slices).

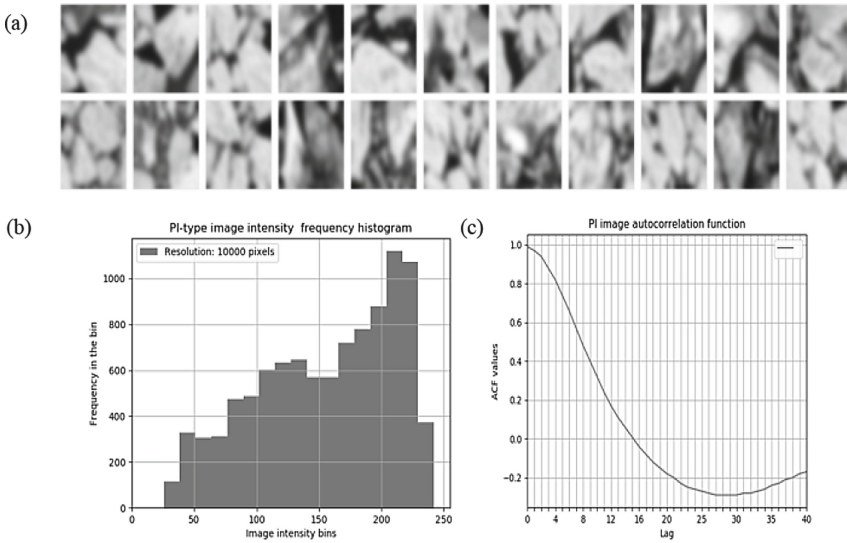


**Fig. 4.** Class “Pack Ice” (PI). (a) Typical sample images from the PI-class. (b) Intensity histogram plotted over the entire typical image from the PI-class. (c) Typical autocorrelation function of PI-image (averaged over different slices).

### 2.3 Description of the D-Classicator Used

In practice, the amount of power available to developers and researchers for training Data Set with aerial survey data is affected by legal restrictions. In particular, special licenses are usually required to use high-resolution remote sensing data. A significant number of modern airborne video sensors fall under this limitation. Thus, the Data Set with aerial imagery data available to a particular developer-researcher may by no means always be of significant (more than a thousand samples per class) power. In the present work, we assume that for training classifier D, researchers have access to a Data Set of relatively small power. Since the dimensionality of feature space is relatively small, and the images in Data Set have a relatively large correlation radius (8 or more pixels), the samples of the same class will relatively “smoothly” differ from each other by the metric of  $\mathbf{F}$ -space. Under these conditions, it is logical to use a conventional and very computationally economical multi-class SVM (MC-SVM) as a D-classifier [27]. For comparison, a DL-classifier was also used: ResNet20 [28]. During training, in order to ensure control of the generalization ability of the classifiers, the standard Cross Validation scheme was used, in the LOO (leave-one-out) variant. For the MC SVM classifier, given the multiclass formulation of the problem, a one-vs-rest strategy was used.

## 3 Results

The results of the numerical studies are summarized in Tables 1–3. The main information is contained in Table 1. Here we accumulate the results, which were shown on the test Data Set by classifiers based on MC SVM and Resnet20. A standard set of metrics was used to evaluate the classification results: precision, recall, and f1-score. The table shows that in the experiments, exactly 24 samples from each class were used at the test stage.

**Table 1.** The basic metrics values on the test Data Set.

Image class	Method	Precision	Recall	f1-score	Support
Open space (OS)	SVM	1.0	0.96	0.98	24
	Resnet20	0.96	1.00	0.98	24
Marginal ice zone (MIZ)	SVM	0.96	1.00	0.98	24
	Resnet20	0.92	1.00	0.96	24
Pack ice (PI)	SVM	1.00	1.00	1.00	43
	Resnet20	1.00	0.93	0.96	43

Tables 2 and 3 contain the so-called confusion matrix for classifier implementations by MS SVM and Resnet20 schemes, respectively. In general, the classification results are quite good. A more detailed analysis of the results is given in the Discussion section.

**Table 2.** Confusion matrix for MC-SVM.

Image class	OS	MIZ	PI
Open space (OS)	23	0	1
Marginal ice zone (MIZ)	0	24	0
Pack ice (PI)	0	0	42

**Table 3.** Confusion matrix for ResNet20.

Image class	OS	MIZ	PI
Open space (OS)	24	0	0
Marginal ice zone(MIZ)	0	24	0
Pack ice (PI)	1	2	40

## 4 Discussion

As follows from Tables 1–3, the classifiers built according to different schemes, taking into account the low power of the Data Set, showed very decent results. At the same time, the classifier based on MC SVM is slightly superior in all parameters to the classifier based on ResNet20. This is due to the insufficient power of the Data Set to provide full training of the DL-classifier, in this case, ResNet20. It is known that the training of DL-classifiers, for example based on Deep Convolutional Neural Network, requires a Data Set of considerable power (more than 1000 instances for each class). This is due to the fact that DL-classifier is a very complex model, which depends on tens of thousands (and more) parameters. It follows from machine learning theory [29] that model complexity should grow “slowly” as the size of the training Data Set increases. Therefore, on small Data Sets, the DL-classifier simply does not have time to be trained, due to the mismatch in the complexity of the classifier and the Data Set. Analysis of confusion matrixes shows that MC SVM made only 1 mistake, confusing classes PI and OO. This is probably due to the fact that these classes, despite their many differences, have in common: a significant part of the surface, in both cases, may occupy a coherent, texturally homogeneous array: a water surface (OO-class) or a solid ice slab (PI-class). The ResNet20-based classifier made three errors. All errors are related to incorrect classification of samples from the PI-class. The reason for the errors: insufficient capacity of the Data Set to fully train the ResNet20-based classifier.



## 5 Conclusions

The paper suggests a new method for classifying the sea-ice floe size distribution type based on the use of low-quality video footage. Low quality of video footage is quite typical for high latitude conditions, where most of the year a set of complex meteorological factors negatively affects the quality of aerial photography. That is why ice reconnaissance data processing should be able to compensate the negative influence of meteorological factors on the quality of ice surface imagery. In other words, ice reconnaissance data processing should be able to estimate with high reliability the sea-ice floe size distribution type, because this estimation is one of the main results of ice reconnaissance. The sea-ice floe size distribution type classification method proposed in the article has high robustness to noises and distortions of the source video material, which makes it an effective means of overcoming the negative influence of a complex high latitude meteorological environment. The simulation results showed high reliability in solving the task of estimating the sea-ice floe size distribution type, which the proposed method provides under the condition of highly noisy and distorted source data. The proposed method is economical in the computational sense and, therefore, it can be implemented in software on a medium- and low-power computing platform placed on board a small-sized ice reconnaissance UAV.

## References

1. Pershin, N.V.: Rational design of sailing routes taking into account hydro meteorological conditions. *Sci. Notes Russ. State Hydrometeorological Univ.* **52**, 62–66 (2018)
2. Mironenko, A.A.: Gradient model of the program motion of the ship. *Navig. Hydrography* **34**, 35–42 (2012)
3. Kalinina, N.V.: Influence of navigation characteristics of ice on ice modesty. *Transp. Syst.* **3**(6), 37–44 (2017)
4. Horvat, C., Tziperman, E.: The evolution of scaling laws in the sea ice floe size distribution. *J. Geophys. Res. Oceans* **122**, 7630–7650 (2017). <https://doi.org/10.1002/2016JC012573>
5. Rothrock, D., Thorndike, A.: Measuring the sea ice floe size distribution. *J. Geophys. Res.* **89**(C4), 6477–6486 (1984). <https://doi.org/10.1029/JC089iC04p06477>
6. Alberello, A., et al.: Brief communication: Pancake ice floe size distribution during the winter expansion of the Antarctic marginal ice zone. *Cryosphere* **13**(1), 41–48 (2019). <https://doi.org/10.5194/tc-13-41-2019>
7. Zhang, J., Schweiger, A., Steele, M., Stern, H.: Sea ice floe size distribution in the marginal ice zone: theory and numerical experiments. *J. Geophys. Res. Oceans* **120**(5), 3484–3498 (2015). <https://doi.org/10.1002/2015jc010770>
8. Lu, P., Li, Z.J., Zhang, Z.H., Dong, X.L.: Aerial observations of floe size distribution in the marginal ice zone of summer Prydz Bay. *J. Geophys. Res.* **113**(C2) (2008). <https://doi.org/10.1029/2006jc003965>
9. Toyota, T., Takatsuji, S., Nakayama, M.: Characteristics of sea ice floe size distribution in the seasonal ice zone. *Geophys. Res. Lett.* **33**(2). <https://doi.org/10.1029/2005gl024556> (2006)
10. Toyota, T., Haas, C., Tamura, T.: Size distribution and shape properties of relatively small sea-ice floes in the Antarctic marginal ice zone in late winter. *Deep Sea Res. Part II* **58**(9–10), 1182–1193 (2011). <https://doi.org/10.1016/j.dsr2.2010.10.034>
11. Stern, H.L.: On reconciling disparate studies of the sea-ice floe size distribution. *Elem. Sci. Anth.* **6**, 49 (2018). <https://doi.org/10.1525/elementa.304>

12. Isanin, N.: Ice cohesion. In: *Naval Encyclopedic Handbook*, vol. 2, p. 403. Shipbuilding, Leningrad (1987)
13. Leshkevich, G.A.: Machine classification of freshwater ice types from landsat—I digital data using ice albedos as training sets. *Remote Sens. Environ.* **17**(3), 251–263 (1985)
14. Leshkevich, G.A., Nghiem, S.V.: Satellite SAR remote sensing of Great lakes ice cover, part 2. Ice classification and mapping. *J. Great Lakes Res.* **33**(4), 736–750 (2007)
15. Nghiem, S.V., Leshkevich, G.A.: Satellite SAR remote sensing of Great Lakes ice cover, part 1. Ice backscatter signatures at C-band. *J. Great Lakes Res.* **33**(4), 722–735 (2007)
16. Anisiforov, A., Dubgorn, A., Lepekhin, A.: Organizational and economic changes in the development of enterprise architecture. *E3S Web Conf.* **110**, 02051 (2019)
17. Gedney, R.T., Mark, H.: *Great Lakes All-weather Ice Information System*. NASA Technical Memorandum NASA TM X-71815, pp. 22161. National Technical Information Service, Springfield, VA (1975)
18. Orlova, V., Ilin, I., Shirokova, S.: Management of port industrial complex development: environmental and project dimensions. *MATEC Web Conf.* **193**, 05055 (2018)
19. Kamangir, H., Maryam, R., Dugan, D., John, D.P., Geoffrey, C.F.: Detecting ice layers in radar images with deep learning. In: *IGARSS* (2018)
20. Birnbaum, G., Lüpkes, C.: A new parameterization of surface drag in the marginal sea ice zone. *Tellus Ser. A* **54**(1), 107–123 (2002). <https://doi.org/10.1034/j.1600-0870.2002.00243.x>
21. Ilin, I., Kalinina, O., Iliashenko, O., Levina, A.: IT-architecture reengineering as a prerequisite for sustainable development in Saint Petersburg urban underground. *Procedia Eng.* **165**, 1683–1692 (2016)
22. Smith, D., Barrett, E., Scott, J.: Sea-ice type classification from ERS-1 SAR data based on grey level and texture information. *Polar Rec.* **31**(177), 135–146 (1995). <https://doi.org/10.1017/S0032247400013632>
23. Shen, X., Zhang, J., Meng, J., Zhang, J., Ke, C.: Sea ice type classification based on random forest machine learning with Cryosat-2 altimeter data. In: *2017 International Workshop on Remote Sensing with Intelligent Processing (RSIP)* (2017). <https://doi.org/10.1109/rsip.2017.7958792>
24. Bateson, A.W., Feltham, D.L., Schroeder, D., Hosekova, L., Ridley, J.K., Aksenov, Y.: Impact of sea ice floe size distribution on seasonal fragmentation and melt of Arctic sea ice. *The Cryosphere* **14**(2), 403–428 (2020). <https://doi.org/10.5194/tc-14-403-2020>. <http://centaur.reading.ac.uk/89246/>
25. Bril, A., Kalinina, O., Ilin, I.: Small innovative company’s valuation within venture capital financing of projects in the construction industry. *MATEC Web Conf.* **106**, 08010 (2017)
26. Timofeev, A.V.: Detection of a small target object in blurry images affected by affine distortions. *Sci. Tech. J. Inform. Technol., Mech. Optics* **21**(2), 206–224 (2021). <https://doi.org/10.17586/2226-1494-2021-21-2-206-224>
27. Didenko, N., Skripnuk, D., Kikkas, K., Kalinina, O., Kosinski, E.: The impact of digital transformation on the micrologistic system, and the open innovation in logistics. *J. Open Innov.: Technol., Market, Complexity* **7**(2), 115 (2021)
28. He, K., Zhang, X., Ren, S., Sun, J.: Deep Residual Learning for Image Recognition. In: *2016 IEEE Conference on Computer Vision and Pattern Recognition (CVPR)* (2016). <https://doi.org/10.1109/cvpr.2016.90>
29. Hastie, T., Tibshirani, R., Friedman, J.: *The Elements of Statistical Learning*. Springer New York, New York, NY (2009)